Cell Reports
Physical Science

CellPress
OPEN ACCESS

Article

Single emulsion drops for photocatalytic water splitting as a membrane-free approach to product separation

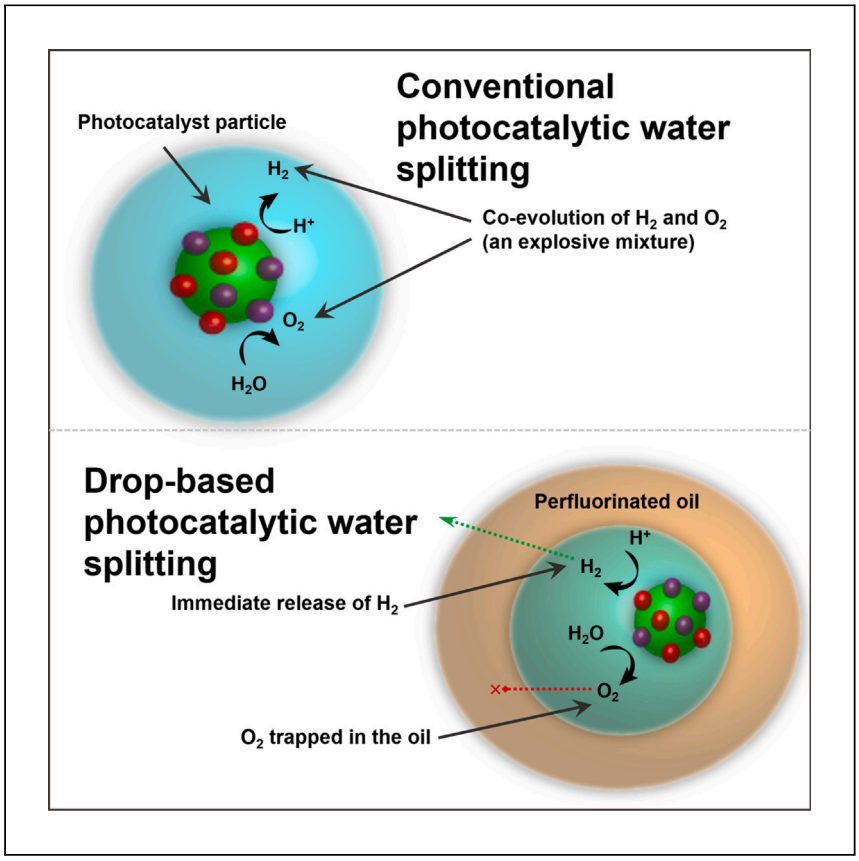

Savant et al. demonstrate inherent separation of hydrogen and oxygen through drop-based photocatalytic water splitting by employing perfluorinated oils to capture evolved oxygen while releasing hydrogen with a stream purity of greater than 99%. The captured oxygen dissolved in the oil is released by heating when required.

Sangram Ashok Savant, Gaia De Angelis, Swarnava Nandy, Esther Amstad, Sophia Haussener

sophia.haussener@epfl.ch

Highlights

Inherent separation of H_2 and O_2 in drop-based photocatalytic water splitting

Trapping of evolved O_2 in perfluorinated oil owing to its high oxygen solubility

Demonstration of successful capture of O_2 while releasing H_2 in drop-based systems

Microfluidic device allows significant decreased residence time of photocatalyst

Savant et al., Cell Reports Physical Science 5, 101755
January 17, 2024
https://doi.org/10.1016/j.xcrp.2023.101755

Please cite this article in press as: Savant et al., Single emulsion drops for photocatalytic water splitting as a membrane-free approach to product separation, Cell Reports Physical Science (2023), https://doi.org/10.1016/j.xcrp.2023.101755

Cell Reports
Physical Science

CellPress
OPEN ACCESS

Article

Single emulsion drops for photocatalytic water splitting as a membrane-free approach to product separation

Sangram Ashok Savant,[1] Gaia De Angelis,[2] Swarnava Nandy,[1,3] Esther Amstad,[2] and Sophia Haussener[1,4,*]

SUMMARY

The coevolution of hydrogen and oxygen during photocatalytic water splitting presents a challenge for efficient product separation. Here, we demonstrate membrane-free, drop-based photocatalytic water splitting with inherent product separation and competitive production rates. Drops composed of an aqueous solution containing a mediator and photocatalysts are surrounded by perfluorinated oil made (1) by mechanical agitation of a bulk mixture or (2) within a microfluidic device. The high oxygen solubility of the oil allows for inherent trapping of oxygen while immediately releasing hydrogen. We achieve average solar-to-hydrogen efficiencies of 0.024% ± 0.001% in the conventional suspension approach, 0.016% ± 0.002% in the bulk emulsion system, and 0.046% ± 0.008% if drops are irradiated in the microfluidic device. A three orders of magnitude decrease in the residence time of photocatalysts with a 1.34 times increase in production rate is possible in the microfluidic drop approach when compared to conventional suspensions. Oxygen is trapped and easily released by heating the oil effluent at 343 K.

INTRODUCTION

Hydrogen as an energy vector can help to diversify the present energy mix and overcome the dependence on fossil fuels.[1–3] Photocatalytic water splitting is a promising pathway to generate green hydrogen and oxygen by utilizing sunlight and an abundant, nontoxic reactant, i.e., water, converting it with the aid of semiconducting photocatalysts.[4–7] The approach has been predicted to be economically viable.[8] Metal oxides have been widely used as photocatalysts, exhibiting high quantum efficiency but utilizing only ultraviolet (UV) irradiation owing to their wide band-gap energies.[9–12] More recently, several narrow band-gap nonoxides were reported for hydrogen and/or oxygen gas evolution reactions via one-step or two-step (i.e., Z-scheme) photoexcitation.[7] In the practical implementation, immediate product separation is desired but not necessarily given when implemented via particle suspension batch reactors. New methods for the separation of the mixture of gaseous products are required.[3,5]

In laboratory-scale experiments, photocatalytic overall water splitting has typically been performed in a single compartment vessel, leading to the coevolution of H_2 and O_2 gases. Only few reports include efficient methods to separate these products, and they typically require Z-scheme systems using water-soluble redox mediators, where hydrogen evolution and mediator oxidation occur in one compartment

[1]Laboratory of Renewable Energy Science and Engineering, Institute of Mechanical Engineering, EPFL, Station 9, 1015 Lausanne, Switzerland

[2]Soft Materials Laboratory, Institute of Materials, EPFL, Station 12, 1015 Lausanne, Switzerland

[3]Present address: Research Initiative for Supra-Materials (RISM), Shinshu University, 4-17-1 Wakasato, Nagano 380-8553, Japan

[4]Lead contact

*Correspondence: sophia.haussener@epfl.ch

https://doi.org/10.1016/j.xcrp.2023.101755

and oxygen evolution and mediator reduction occur in the other compartment. The compartments are separated by a semipermeable membrane. In one of the most efficient demonstrations, Ru/$SrTiO_3$:Rh, $BiVO_4$ and $[Co(bpy)_3]^{3+/2+}$ were used as a hydrogen evolution photocatalyst (HEP), oxygen evolution photocatalyst (OEP), and redox mediator, respectively, where reduced and oxidized species of the mediator were allowed to pass between the two vessel compartments through a membrane.[13] However, trace amounts (~17 μL) of H_2 were detected in the oxygen compartment, as the H_2 molecule still permeated through the membrane. Unfortunately, membrane approaches allow the separation of product gases only in Z-scheme designs, requiring two photocatalysts and ruling out the possibility of intrinsic product separation in a one-step overall water-splitting reaction involving single photocatalysts. Suitable methods are needed that do not rely on the selective transportation properties of membranes, that enable separation of gaseous mixtures for both single- and two-step overall water splitting, and that reliably and with high purity separate the product gases.

Emulsion drops are often used to conduct biological and chemical screening tests.[14–16] These drop-based screening tests are frequently performed using aqueous drops dispersed in perfluorinated oils.[17] These oils have a high oxygen solubility (i.e., oxygen solubility in HFE-7500 is ~100 mL/L at standard conditions, ~25 times higher than water[18]). In addition to the high oxygen solubility, perfluorinated oils lack a greasy nature, unlike some of their hydrocarbon counterparts, making them ideal for the formation of water-in-oil emulsions.[19] When combined with appropriate surfactants, perfluorinated oil/water systems display a low interfacial tension, facilitating the stable formation of emulsions within microchannels.[19] Consequently, in 1 L oil, we can dissolve 4,460 μmol O_2. Considering the best-performing oxygen evolution activity of 40–50 μmol h^{-1} for BiVO4:Mo or Au/CoO_x/$BiVO_4$, the holding capacity of the oil after extended hours of illumination in a batch system would be sufficient.[8] Contrary to oxygen, hydrogen is generally not soluble in perfluorinated oils. With hydrogen being a nonpolar molecule and perfluorinated oils being nonpolar solvents due to the strong electronegativity of fluorine atoms, the hydrogen solubility is very low.[20,21] For reference, the hydrogen solubility in fuel oils is as low as 0.02–0.06 mol fraction in the liquid phase of the oil.[20] Therefore, the utilization of HFE in photocatalytic water splitting by forming single emulsion drops can open a new route for the inherent separation of H_2 and O_2, not requiring the complexity of designing different kinds of reactors involving selective transportation properties of membranes.[18] The catalyst can be recovered in the drop-based approach by centrifuging the emulsions and recovering and washing the catalyst before reinjecting it into the system.

In this work, we demonstrate the use of water-in-oil single emulsions for photocatalytic overall water splitting under visible-light irradiation. Specifically, state-of-the-art photocatalysts (Pt-loaded $SrTiO_3$:Rh,La and/or WO_3 as HEP and/or OEP) are dispersed in an aqueous mediator (aq. $FeCl_3$/$FeCl_2$) and emulsified in HFE oil before being illuminated with light, either in batch or in a microfluidic (MF) device/reactor.

RESULTS AND DISCUSSION

Two cases: Drop emulsions and microfluidics

We performed photocatalytic water splitting by three methods: (1) a conventional suspension (CS) system (Figure 1A), (2) a drop emulsion system (Figure 1B) wherein we encapsulated the semiconductor and aqueous mediator in a drop surrounded by HFE oil (which captures oxygen), and (3) a microfluidic device (Figure 1C) using

Please cite this article in press as: Savant et al., Single emulsion drops for photocatalytic water splitting as a membrane-free approach to product separation, Cell Reports Physical Science (2023), https://doi.org/10.1016/j.xcrp.2023.101755

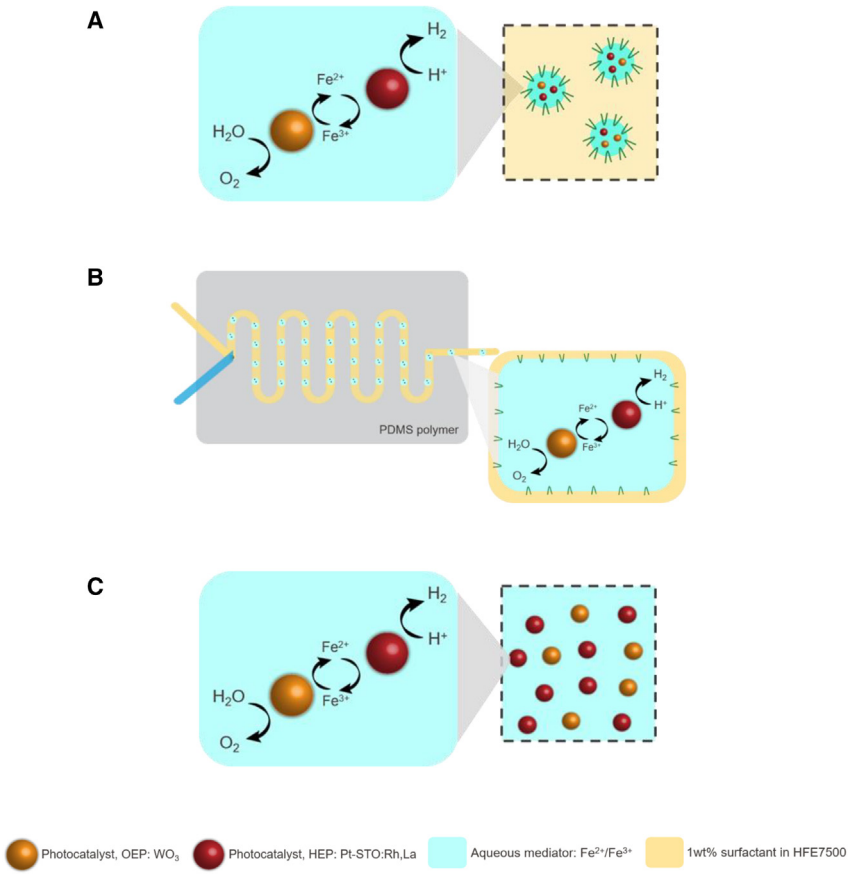

Figure 1. Schematic diagrams for three different approaches employed for water splitting
Schematic diagrams of (A) a conventional suspension system with photocatalyst particles in solution and water-in-oil drops obtained by (B) mechanical agitation and (C) with a microfluidic device. The aqueous drops comprise HEP and OEP particles and a mediator. They are surrounded by HFE containing 1 wt % surfactant. Schematics show two-particle configurations for Z-scheme OWS. Half reactions can be conducted in the same three systems when only HEP or OEP particles are added.

the same aqueous phase and surrounding oil as in case 2 to create monodisperse emulsions and to individually expose them to the illumination. We performed the conventional suspension experiments (case 1) to have a benchmark case with which we compare the other two approaches that have inherent separation capabilities. All three systems can be used to perform half reactions for either the oxygen evolution reaction (OER) and the hydrogen evolution reaction (HER) employing either OEP or HEP particles, respectively, as well as to perform Z-scheme overall water splitting (OWS) employing both sets of semiconductor photocatalysts simultaneously.

Water-in-oil emulsions were prepared either by mechanical agitation (Figure 2B) or with the use of a microfluidic flow-focusing device (Figure 2A), as explained in the supplemental experimental procedures, similar to other reported methods.[22]

Drops formed with microfluidic devices were monodisperse with drop diameters between 91 and 114 μm, averaging at 100 μm, as shown in Figures 2A and 2D. By contrast, drops formed through mechanical agitation were polydisperse with diameters between 10 and 150 μm and a mean of 80 μm, as shown in Figures 2B and 2D.

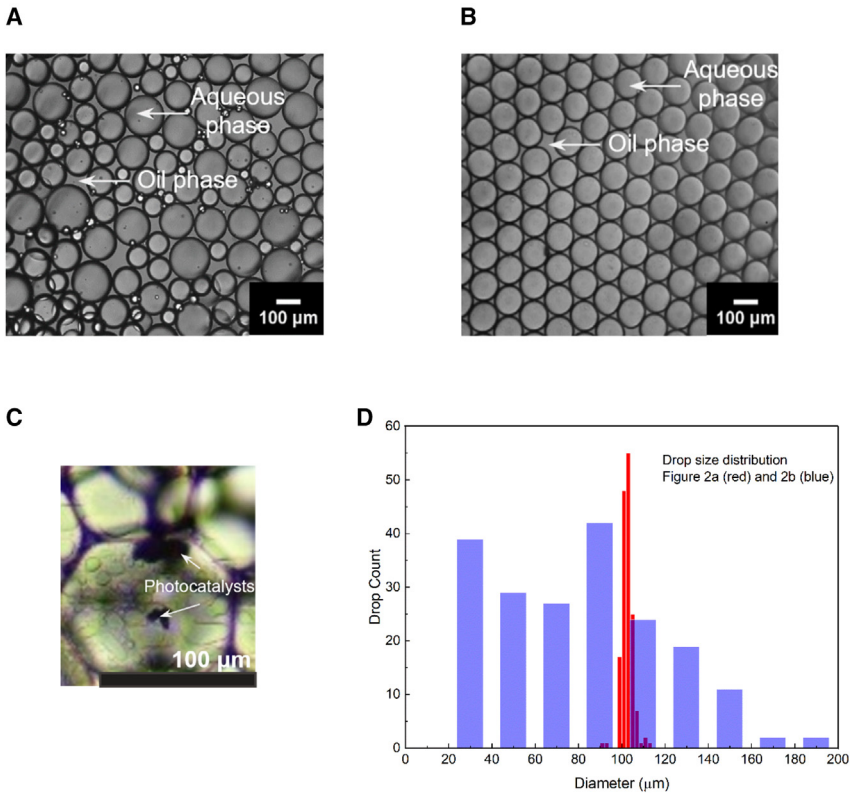

Figure 2. Optical micrographs of drops produced by mechanical agitation of a bulk mixture vs. those produced in microfluidic (MF) devices and their size distribution

Optical micrographs of single water-in-oil emulsion drops made using (A) an MF device (scale bar: 100 µm) and (B) mechanical agitation (scale bar: 100 µm); (C) zoom in of aggregated photocatalyst particles trapped in drops with a diameter of 110 µm (scale bar: 100 µm); and (D) histograms showing the corresponding drop size distribution: red bars represent drops made with an MF device (A), and the blue bars represent drops made by mechanical agitation (B).

Note that photocatalytic particles agglomerated within the aqueous drops, as shown in Figure 2C. This agglomeration was reduced by sonicating the aqueous dispersion before emulsification and by stirring the emulsion, when possible, during the water-splitting reaction.

Most emulsion drops, if not stabilized by surfactants, tend to coalesce to minimize the liquid-liquid interfacial area and therefore the interfacial energy of the system. The presence of high concentrations of salts, such as iron chlorides, and other species in the aqueous phase further reduces the drop stability.[23] Nevertheless, the commercially available Krytox FSH (fluorinated surfactant type H) surfactant, which contains a functionalized carboxylic acid group at the terminal fluoromethylene group, could initially stabilize aqueous drops if they contained the cationic polydiallyldimethylammonium chloride (PolyDADMAC), as shown in Figure S1. However, the iron chloride started to precipitate within 2 h (Figure S2), resulting in unstable emulsions, which prevented an efficient use of this system. To address this limitation, we stabilized the emulsions with a fluorinated block copolymer surfactant, FSH_2J900.[23–26] This surfactant efficiently stabilized the aqueous drops and does not influence the solution pH. However, to produce sufficient amounts of gases to enable their reliable detection, large volumes (in the range of 50–100 mL) of the oil and surfactants are required. To enable the synthesis of the surfactant at

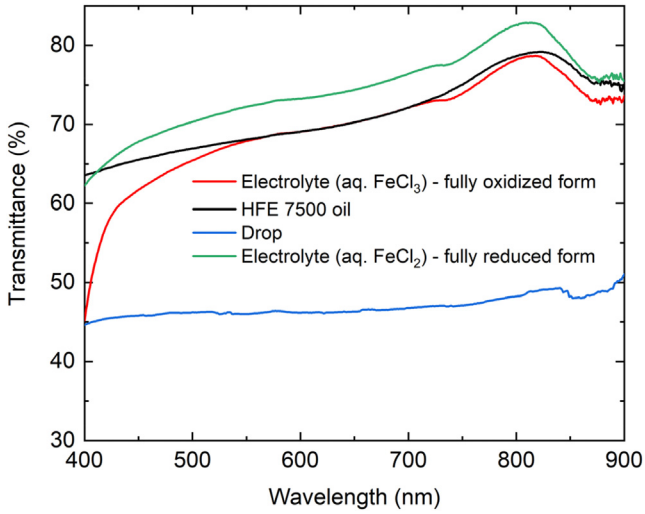

Figure 3. Optical characterization of solutions employed in the three different approaches
Transmittance (%) vs. wavelength (nm) for mediator (4 mM aqueous $FeCl_3$, oxidized form) (red), HFE-7500 (black), emulsions with aqueous drops containing $FeCl_3$ without particles (blue), and mediator (4 mM aqueous $FeCl_2$, reduced form) (green). The transmittance was adjusted for a path length of 25 mm (thickness of our reactor).

sufficiently large scales as required by this application, we adapted the synthesis protocol, as detailed in the experimental procedures.

We performed a UV-visible (UV-vis) spectrometric analysis (400–900 nm irradiation) to characterize the optical behavior of the solutions representative of the three cases and to estimate the scattering losses in the drop emulsions. The transmittance of the individual components (measured in a 12.5-mm-thick cuvette and then adjusted to the reactor thickness of 25 mm) of the conventional suspension system and the emulsion system is shown in Figure 3. Deionized (DI) water was used as reference. The wavelength-averaged transmittance of the mediator solution (in fully reduced and fully oxidized mediator form) varies between 74% and 70%, indicating that 5%–6% variation in transmittance between unconverted and fully converted reactions can be expected. HFE-7500 has a similar transmittance. By contrast, the wavelength-averaged transmittance of water-in-oil emulsions is much lower, 47%. We assign the decreased transmittance to scattering losses caused by the emulsion drops. This transmittance is relatively uniform over the wavelength range. Consequently, we estimate that the relative radiation loss due to scattering in the emulsion (case 2) compared to the conventional suspension (case 1) is 31%, averaging over a wavelength range of 400–900 nm.

To test the influence of the solution system on the photocatalytic water-splitting efficiency, we performed these reactions using Pt-loaded $SrTiO_3$:Rh,La (as HEP) and commercially available tungsten oxide (WO_3) (as OEP). Pt-loaded $SrTiO_3$:Rh,La was prepared using a one-step solid-state reaction (details in the supplemental information).[27] The selection of the photocatalysts was done considering their compatibility as HEP and OEP, stability, and ease of synthesis. $SrTiO_3$ (a widely studied and employed HEP) is a n-type semiconductor with a perovskite-type cubic structure of ABO_3; its susceptibility toward the substitution of dopants at both Sr and Ti sites of the STO crystal lattice makes it a unique material for band-gap engineering.[28,29] The conduction band (CB) and valence band (VB) of $SrTiO_3$ are characterized by the titanium 3d (Ti 3d) and oxygen 2p (O 2p) states, respectively. $SrTiO_3$

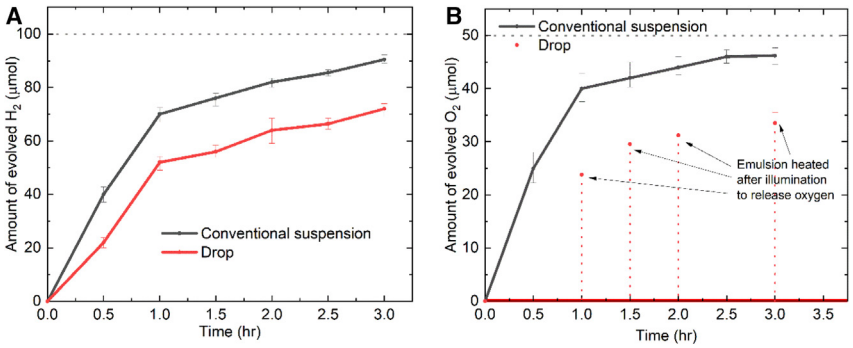

Figure 4. Evolution profile of hydrogen and oxygen half reactions in the conventional suspension vs. the drop approach

(A) Evolution profile of the hydrogen half reaction. The conventional system (case 1) and emulsions (case 2) contain 50 mL 4 mM $FeCl_2$ and 0.1 g Pt-loaded $SrTiO_3$:Rh,La. The horizontal dotted line denotes the maximum possible evolution for the given volume and concentration of mediator.

(B) Evolution profile of oxygen half reaction. The conventional system (case 1) and emulsions (case 2) contain 50 mL 4 mM $FeCl_3$ and 0.1 g WO_3. No oxygen was measured in the emulsion unless the emulsions were heated to 343 K to release the oxygen. This was done for four different experiments with experimental durations of 1, 1.5, 2, and 3 h. Each experiment was repeated 5 times, and the error bars denote the standard deviations of the experiments.

only absorbs UV light (optical band gap of 3.2 eV), and in-gap states can be induced through doping with metal cations to extend the spectral response toward visible light. $SrTiO_3$, when doped with Rh, absorbs visible light via a transition from electron donor levels formed by Rh^{3+} ions to the Ti 3d orbital of $SrTiO_3$, which serves as the CB.[28,30] The formation of anions is suppressed by accommodating both trivalent and tetravalent Rh ions at tetravalent Ti sites. The codoping of La^{3+} ions at Sr^{2+} sites suppresses the formation of oxygen vacancies and improves the photocatalytic activity for H_2 evolution. WO_3 is one of the most commonly used OEPs, being a visible-light-responsive oxide semiconductor. WO_3 is selective to O_2 given its CB and VB positions relative to the two redox reaction potentials.[9] The $Fe^{2+/3+}$ redox mediator was selected for its appropriate potential with respect to the band gaps of the HEP and OEP to undergo reduction and oxidation in order to shuttle electrons for the required reactions. In addition, $Fe^{2+/3+}$ are readily complexed with 2,4,6-Tri(2-pyridyl)-s-triazine, which was essential for colorimetry to determine the concentration of the reduction/oxidation species available.[31]

Half reactions: Conventional suspension vs. drop emulsion system

To assess the influence of the system on the photocatalytic water-splitting reactions, we first performed the two-half reactions independently. The catalyst-containing solutions were illuminated with a xenon lamp (300 W) and the evolved gases analyzed with a gas chromatograph (GC), as detailed in the "photocatalysis setup" section. Tested irradiation intensities were at reference conditions 2,028 W/m^2 for the conventional suspension and batch emulsion.

Figure 4A shows the comparison of the evolution of the hydrogen half reaction in a batch reactor for conventional suspension systems (case 1) vs. emulsions (case 2). In conventional batch systems, we observe an initial increase in the H_2 evolution rate that we assign to the availability of Fe^{2+} ions in the initial phase of the experiment and the higher transmittance of $FeCl_2$ compared to that of $FeCl_3$. The evolution rate decreases with decreasing concentration of Fe^{2+} ions in the surroundings and with the consequent increase in Fe^{3+} ions, which translates into a lower

transmittance of the solution. The gas evolution continues until all Fe^{2+} ions have been converted to Fe^{3+} ions. Even though the reaction was not yet complete after 3 h, we stopped the experiment at this point because the evolution rates became slow (below 9 μmol/h for H_2 and below 5 μmol/h for O_2), as shown in Figure 4A. Within this duration, the conventional suspension system produced 90.4 μmol H_2. The hydrogen production rate was lower in the emulsion system, where we produced in the same time only 72 μmol H_2. We assign the lower H_2 production of the emulsion system to scattering losses caused by the drops, as detailed in the optical characterization (Figure 3). Indeed, the amount of H_2 generated within 3 h is only 20.4% below that produced in batch systems, whereas the transmittance of the emulsion is 31% lower than that of the batch system. The drops can be considered mini-reactors of approximately 100 μm diameter (Figure 2), which can be expected to provide an advantage of shorter diffusion lengths along with ease of mass transport during the water-splitting reactions.

The key reason to implement a drop-based approach is to capture the oxygen in the HFE-7500 oil. To ensure that the oil does not contain significant amounts of oxygen prior to the experiment, we preheated the oil before illumination. In the conventional batch system, we continuously monitored the oxygen evolution. We produced 46.22 μmol O_2 after 3 h illumination. In the emulsion-based system, we quantified the amount of oxygen in the oil after the emulsions had been illuminated for 1, 1.5, 2, and 3 h by subsequent heating of the oil to 343 K to release the trapped oxygen. Each data point is a separate experiment run for either 1, 1.5, 2, or 3 h. The emulsion system produced 33.5 μmol O_2 within 3 h. This value is approximately 13 μmol (27.52%) below that produced in batch processes. We again assign the lower values to optical losses, i.e., the light scattering of the drops, while improved mass transport is expected compared to the conventional suspension system. The hydrogen-to-oxygen evolution rates of the two half reactions are at a ratio of 1.93:1, indicating that there are no significant side reactions. There was no evolution of oxygen during the experiments (within detection limits of the GC) represented by the solid red line at 0 μmol O_2. Also, there was no hydrogen detected (within detection limits of the GC) during the heating of the emulsion to extract oxygen. This indicates that the separated hydrogen and oxygen streams are pure (>99.99%).

Z-scheme reactions: Conventional suspension vs. drop emulsion system

We performed Z-scheme water-splitting experiments in conventional suspension systems (case 1) and in emulsions (case 2) to demonstrate their operability as Z-schemes and to quantify the performance. We implement the same set of photocatalysts, namely Pt-loaded $SrTiO_3$:Rh,La for HER and WO_3 for OER, with a suitable aqueous solution containing a mixture of $FeCl_2$ and $FeCl_3$. As observed in Figure 5A, after 3 h illumination, we evolve 49.6 μmol oxygen and 98.3 μmol hydrogen, resulting in a solar-to-hydrogen efficiency of 0.024% ± 0.001% in the conventional suspension system. After approximately 2 h illumination, we reached a steady state where the ratio of hydrogen-to-oxygen production was 1.98:1, which is close to the theoretical ratio of 2:1. This corresponds to around 90% of the maximum theoretical limit thanks to the constant stirring of the solution. Note that the photocatalysts (WO_3 and Pt-loaded $SrTiO_3$:Rh,La) could be prone to degradation over time, specifically to the detachment of the cocatalyst (Pt).[29,30,32]

The gas evolution was slightly lower in the emulsion system; within 3 h of illumination, we produced 41.11 μmol oxygen at a rate of 13.71 μmol/h and 72.23 μmol hydrogen at a rate of 24.11 μmol/h over 3 h (H_2/O_2 ratio of 1.76:1), resulting in a solar-to-hydrogen efficiency of 0.016% ± 0.002%, as shown in Figure 5B. Consistent

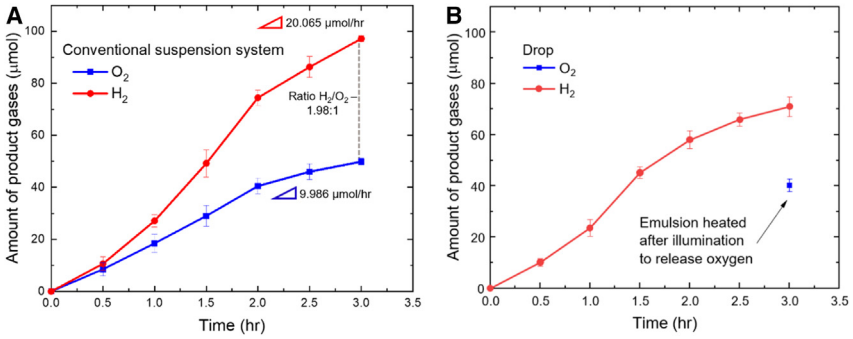

Figure 5. Evolution profile of Z-scheme water splitting in the conventional suspension vs. the drop approach

(A) Evolution profile of Z-scheme water-splitting reaction in a conventional suspension system (case 1). The suspension is based on 50 mL of an aqueous solution containing 4 mM $FeCl_2/FeCl_3$, Pt-loaded $SrTiO_3$:Rh,La and WO_3 photocatalysts (0.05 g each).

(B) Evolution profile of Z-scheme water-splitting reaction in an emulsion system (case 2). The drops are made from 50 mL of an aqueous solution containing a 4 mM $FeCl_2/FeCl_3$ mixture, Pt-loaded $SrTiO_3$:Rh,La, and WO_3 (0.05 g each). They are contained in HFE oil comprising a surfactant. The emulsion was heated after illumination to release the trapped oxygen. Each experiment was repeated 5 times, and the error bars denote the standard deviations of the experiments.

with what has been observed for the half reactions, the emulsion system has a 20%–25% lower hydrogen production compared to the conventional suspension system, likely due to scattering losses but improved mass transport.

Microfluidic device experiments and comparison

While the tested irradiation intensities were at reference conditions 2,028 W/m^2 for the conventional suspension and batch emulsion, we obtained 5,000 W/m^2 for the microfluidic device. The microfluidic device experiments were repeated 5 times, and the measurements have been averaged over the 5 runs in Figures 6B and 6C. Error bars are also shown for the other experiments. This difference in average irradiation intensity resulted from both devices being operated at the same focal plane but with different reactor areas (50 vs. 0.8 cm^2, with the irradiation intensity and flux map as shown in Figure 7). To compare the two systems, experiments with the conventional suspension reactor were also done in front of this focal plane to reach 5,000 W/m^2.

As seen in Figure 6A, for the experiments performed in a batch reactor, we observe the highest hydrogen evolution in Z-scheme in the conventional suspension system of 0.491 μmol H_2/μmol Fe^{2+} against a half-reaction evolution in the conventional suspension system of 0.44 μmol H_2/μmol Fe^{2+}, followed by a Z-scheme reaction evolution in the emulsion system of 0.37 μmol H_2/μmol Fe^{2+} and a half reaction in the emulsion system 0.35 μmol H_2/μmol Fe^{2+}. The highest oxygen evolution of 0.242 μmol O_2/μmol Fe^{3+} is observed in Z-scheme in the conventional suspension system followed by a half-reaction evolution in the conventional suspension system of 0.231 μmol O_2/μmol Fe^{3+}, followed by a Z-scheme reaction evolution in the emulsion system of 0.205 μmol O_2/μmol Fe^{3+} and a half reaction in the emulsion system 0.175 μmol O_2/μmol Fe^{3+}.

The evolution of product gases is slightly higher in the Z-scheme compared to the half reactions. In Z-scheme systems, the redox mediators reach steady state sufficiently fast for OER and HER to have the corresponding mediator ions available, after which their concentration stays constant, in contrast to the half reactions where the sacrificial agents available for OER and HER reduce with time. The emulsions

Please cite this article in press as: Savant et al., Single emulsion drops for photocatalytic water splitting as a membrane-free approach to product separation, Cell Reports Physical Science (2023), https://doi.org/10.1016/j.xcrp.2023.101755

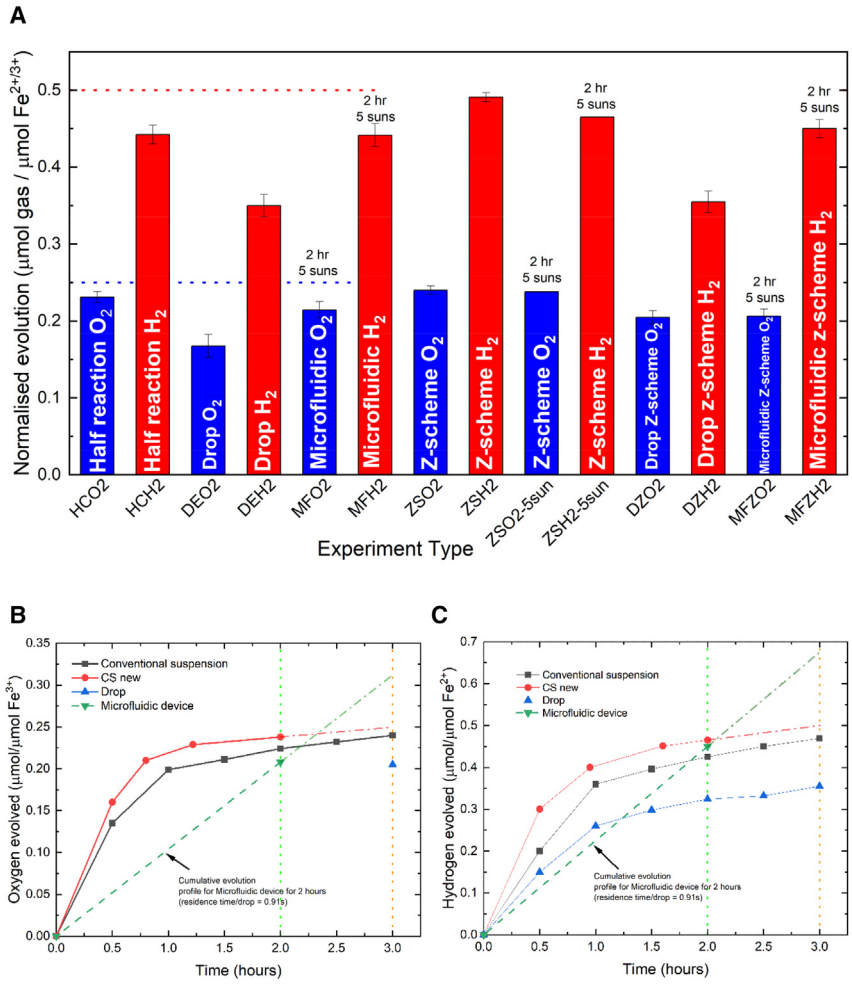

Figure 6. Normalized evolution plots for Z-scheme experiments for all the three approaches: conventional suspension, drops, and MF device

(A) Normalized evolution of product gases for a given concentration of mediator for different systems. The blue and red colors denote the oxygen and hydrogen evolution experiments. If not indicated otherwise, the data are for a 3 h experiment at 2 suns. The red and blue horizontal dotted lines show the maximum extractable hydrogen and oxygen, respectively, for a given concentration of mediator in the Z-scheme experiments (6 bars on the left side). Each experiment (except the ZSO2–5sun and ZSH2–5sun) was repeated 5 times, and the error bars denote the standard deviations of the experiments.

(B and C) Normalized (B) oxygen and (C) hydrogen evolution plots of experiments performed in MF devices (case 3), drops (case 2), and conventional suspensions (case 1) against total duration of the experiment. The particle concentration is 0.1 g/50mL mediator aqueous solution containing 4 mM $FeCl_2/FeCl_3$. Conventional suspensions and emulsions are illuminated at 2,028 W/m^2 (=2 suns), and with the exception of the conventional suspension (CS new) experiment done at 5,000 W/m^2 (=5 suns) (red dashed line), the MF system operates at 5,000 W/m^2. The dot-dash lines for the MF device experiments are an extrapolation (linear) to an experiment time of 3 h to compare against the batch experiments. The corresponding normalized plots of (B) and (C) for half reactions are summarized in Figures S6A and S6B.

suffer from additional scattering losses compared to the conventional suspension system, leading to a further reduction of the evolved product gases.

Emulsions produced with microfluidic devices allow for direct light exposure of the photocatalysts within the microfluidic device, as typically one drop is passing

Please cite this article in press as: Savant et al., Single emulsion drops for photocatalytic water splitting as a membrane-free approach to product separation, Cell Reports Physical Science (2023), https://doi.org/10.1016/j.xcrp.2023.101755

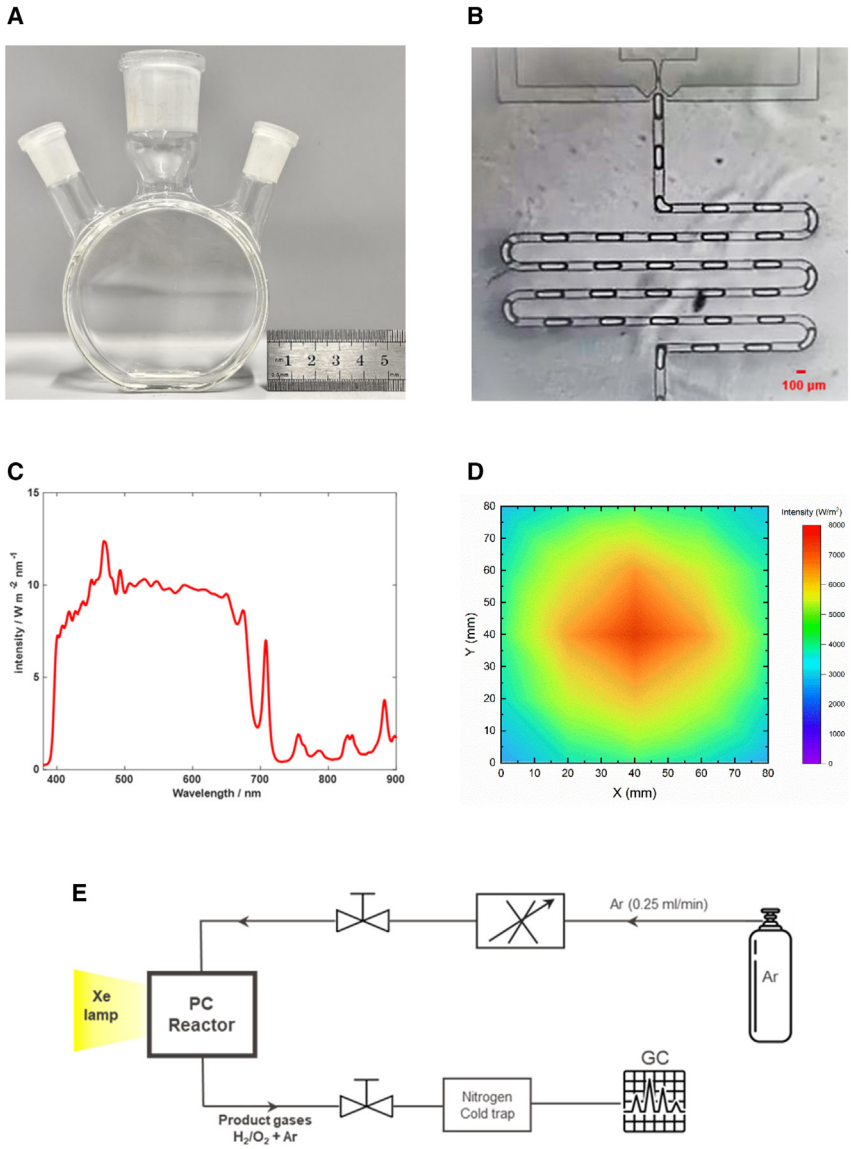

Figure 7. Details of the experimental setup and the lamp used to carry out the photocatalytic reactions

(A) The Pyrex vessel/reactor used for experiments (scale bar: 5 cm); (B) micrograph of the MF device (producing emulsions) used for the MF reactor experiments (right) (scale bar: 100 µm); (C) spectrum of 300 W Xe lamp with λ >400 nm; (D) the flux map of the Xe lamp in the focal spot where the conventional suspension and emulsion reactor is put; and (E) schematic of the experimental setup for measuring the evolved product gases (H_2 and O_2) for the photocatalytic water-splitting reactor.

through the channel at the time (see Figure 7B and Video S1), in contrast to the parasitic scattering observed in the batch emulsions. The half-reaction experiments in the microfluidic device yielded H_2 and O_2 production rates of 0.44 and 0.21 µmol/µmol $Fe^{2+/3}$, respectively. The Z-scheme experiments yielded hydrogen evolution rates of 0.45 µmol H_2/µmol Fe^{2+} and an oxygen evolution of 0.206 µmol O_2/µmol Fe^{3+}. Microfluidic devices performed nearly as well as the conventional suspension at significantly faster residence times (~seconds vs. ~ hours) and as a flow system (vs. batch for the conventional suspension). The microfluidic device offers a competitive performance to conventional

suspension systems, but control over the amount of photocatalyst per drop is challenging.

Even though the residence time of each drop within the microfluidic channel was very short—0.9 s compared to ~hours—0.44 μmol/μmol Fe^{2+} H_2 and 0.21 μmol/μmol Fe^{3+} O_2 were produced in 2 h. These values correspond to a solar-to-hydrogen efficiency of 0.046% ± 0.008% for the microfluidic device. Extrapolating the performance of the microfluidic devices to 3 h, we estimate a hydrogen evolution of about 0.675 μmol H_2/μmol Fe^{2+} and an oxygen evolution of 0.316 μmol O_2/μmol Fe^{3+} vs. the best-performing batch system hydrogen evolution of about 0.491 μmol H_2/μmol Fe^{2+} and an oxygen evolution of 0.242 μmol O_2/μmol Fe^{3+}. The production rates of H_2 and O_2 gases after 3 h operation were therefore improved 1.34 times if drops were individually illuminated within a microfluidic channel compared to those that have been illuminated in batch in suspension (at 5 suns), as shown in Figures 6B and 6C.

In Figures 6B and 6C, the red dashed line represents conventional suspension experiments done at an average intensity of 5,000 W/m^2 (or 5 suns) to offer a point of comparison against the same intensity used in the microfluidic device experiments. As expected, we observe a faster progression of the reaction at 5 suns compared to 2 suns where similar product gas evolutions are already achieved in 1.3 h compared to 3 h. We observe, similarly to the literature, that the reaction rate linearly depends on the light intensity (in the here tested range of 0–5 kW/m^2).[33,34] The overall time of experiments needed by the microfluidic device to reach the same evolution of products as the conventional system is 1.33 times shorter.

To assess the influence of the residence time of the drops within the microfluidic channel on the gas production, we increased the injection flow rate (Figure S5). If the continuous oil phase is injected into the microfluidic device at a rate of 1,000 μL/h, the residence time (i.e., the time for which the drop encapsulating the photocatalyst and mediator was exposed to illumination for both oxygen and hydrogen experiments) was 0.92 s. For this residence time, H_2 and O_2 production was achieved at rates of 0.44 and 0.21 μmol/μmol $Fe^{2+/3+}$, respectively, in their respective half reactions in the presence of sacrificial reagents. Variation in the flow rates between 1,000 and 4,000 μL/h, corresponding to residence times between 0.92 and 0.23 s, showed that flow rates of 1,000 and 2,000 μL/h provided long enough exposure to the illumination to complete the half reactions (see also Figures S3; and S4 for the corresponding conversion), while the shorter residence times did not allow for full conversion.

We propose, demonstrate, and compare a drop-based approach for photocatalytic water splitting that allows for intrinsic product gas separation while showing the potential for more controlled and faster reaction rates. Specifically, we performed photocatalytic water splitting by three methods: (1) conventional suspension system as benchmark and emulsions (2) in bulk and (3) in a microfluidic device, all using Pt-loaded $SrTiO_3$:Rh,La and/or WO_3 as HEP/OEP. The emulsions were prepared either by mechanical agitation or in microfluidic devices. The drops encompassed the semiconductor photocatalysts Pt-loaded $SrTiO_3$:Rh,La and/or WO_3 and the mediator, which was either $FeCl_2$ and/or $FeCl_3$ depending on the desired hydrogen or oxygen half reactions or Z-scheme experiments. We demonstrated that the two drop-based systems intrinsically separated the product gases, capturing oxygen in the oil phase (to be released by a heat treatment on demand) while immediately releasing hydrogen. The demonstration achieved pure hydrogen while trapping oxygen effectively in the oil without holding any hydrogen; thus, the product gas stream purity

was in excess of 99.99%. This demonstration was done in a half-reaction approach as well as in a complete Z-scheme approach. Parasitic scattering losses caused by the emulsions reduced the production of hydrogen and oxygen. This drawback of the emulsion systems in batch conditions could be overcome with a microfluidic reactor wherein every single drop encapsulating the mediator and photocatalyst received direct illumination and thus performed better than case 2. The microfluidic system additionally represents a flow system compared to the batch approach of the conventional suspension or emulsion.

The oxygen half reaction for the conventional suspension system yielded an evolution of 46.22 μmol or 0.231 μmol O_2/μmol Fe^{3+} against emulsion systems yielding 33.5 μmol or 0.175 μmol O_2/μmol Fe^{3+}, reaching 94.2% of the maximum limit for the conventional system and 70% in the emulsion system. The difference in the total evolution was again associated with the parasitic scattering losses in the emulsions. The configuration with a microfluidic device overcame these parasitic optical losses, as drops were individually illuminated within microfluidic channels, resulting in a higher evolution of 0.2145 μmol O_2/μmol Fe^{3+}. In microfluidic devices, we reach about 85.8% of the maximum theoretical limit of possible oxygen evolution.

Following a similar trend, the hydrogen half reaction for the conventional suspension system yielded an evolution of 94 μmol or 0.44 μmol H_2/μmol Fe^{2+}, against the emulsion system yielding 72 μmol or 0.35 μmol H_2/μmol Fe^{2+}, achieving about 94% of the maximum theoretical limit for the conventional system and 72% for the emulsion system. The solar-to-hydrogen efficiency for conventional and emulsion systems for the Z-scheme are 0.024% $\pm$ 0.001% and 0.016% $\pm$ 0.002%, respectively (based on 3 h experiments).

The microfluidic device approach with single emulsion drops yielded evolutions of 0.4416 μmol H_2/μmol Fe^{2+}, higher than case 2, as it did not suffer from the parasitic scattering losses. In the microfluidic device, we reached about 88% of the maximum theoretical limit of possible hydrogen evolution. The microfluidic devices yielded a higher solar-to-hydrogen efficiency of 0.046% $\pm$ 0.008% (based on 2 h experiments), which is between 2 and 3 times larger than that of cases 1 and 2. The corresponding theoretical efficiency limit of the combination of photocatalysts and redox mediators for the Z-scheme reaction is calculated to be 3.85%.[8]

We demonstrated the feasibility of emulsion systems in photocatalytic water splitting to effectively separate the product gases. The approach was demonstrated for half reactions with single photocatalysts as well as Z-scheme configurations with two photocatalysts. The emulsion systems allow for omitting the use of complex, semipermeable membranes and their corresponding mechanical and electrochemical challenges. The inferior evolution activity of the emulsion system—mostly resulting from undesired light scattering losses—compared to the conventional suspension approach can be mitigated by illuminating drops within microfluidic devices. Moreover, the microfluidic system continuously produces product in its flow configuration (in contrast to the two batch systems), and by controlling the flow rate in the microfluidic device, we can optimize the illuminated residence time of the semiconductor photocatalyst.

Due to the small channel dimensions, microfluidic devices inherently possess a low throughput. This throughput can be increased by parallelizing microfluidic devices, for example, by connecting the inlets for the inner and outer phases of parallelized devices through large channels that serve as fluid reservoirs. The use of such

reservoirs risks introducing pressure gradients along the parallelized devices, which result in gradients in fluid flow rates that translate into differences in the sizes of the drops formed within different microfluidic devices. This risk can be mitigated by designing sufficiently large reservoirs to ensure that the pressure drop across the entire reservoir is at least 10-fold lower than that in each individual microfluidic channel. A peculiarity of our system is the risk of catalyst agglomeration within these reservoirs, which would risk clogging of the channel. This risk could be minimized by appropriately surface modifying the catalysts and by introducing filters into the inlets of each microfluidic device.

EXPERIMENTAL PROCEDURES

Resource availability

Lead contact

Requests for further information, resources, or materials should be directed to and will be fulfilled by the lead contact, Professor Sophia Haussener (sophia.haussener@epfl.ch), upon reasonable request.

Materials availability

This study did not generate new unique materials.

Data and code availability

The data generated in this study are included in the manuscript and supplemental information and will be made available from the lead contact upon reasonable request.

Photocatalysis setup

The reactor is a Pyrex vessel with a capacity of 100 mL (Figure 7A) with high transmittance (~95% for Pyrex glass; see Figure S5A) for λ >400 nm.[35] The irradiation area of the vessel is 50 cm^2, and the width of the reactor is 25 mm.

The Pyrex reactor is replaced with a microfluidic device (Figure 7B) for the microfluidic experiments and has a total irradiated area of 0.8 cm^2. PDMS (polydimethylsiloxane) is used to produce the microfluidic device as it has a high transmittance (~95% for PDMS; see Figure S5B) for λ >400 nm.[36] Figure S7 shows the optical transmittance of the Pyrex glass as well as the PDMS used in the microfluidic device to ensure its suitability to transparence in the 400–900 nm spectrum.

The xenon lamp is a 300 W lamp λ >400 nm (spectrum seen in Figure 7C and flux map in Figure 7D) with an average intensity of 2,028 W/m^2 over the reactor area of 50 cm^2. The microfluidic device receives an average intensity of 5,000 W/m^2 over an area of 0.8 cm^2 when located at the same focal plane. For some experiments, the conventional system was put closer to the light source to also operate with an average intensity of 5,000 W/m^2. Photocatalytic water splitting was performed using single emulsion drops or a conventional suspension method by dispersing 0.1 g photocatalysts (of HEP or OEP catalyst for the half reactions or in total of HEP and OEP [i.e., 50 mg each] catalyst for the Z-scheme demonstrations) into a 50 mL aqueous solution of Fe^{2+}/Fe^{3+} (each 4 mM). The mixture placed in a Pyrex reaction vessel was stirred with a magnetic stirrer to assist with particle suspension. Evolved gases were analyzed by gas chromatography (with a thermal conductivity detector, 5 Å molecular sieve columns, and argon as carrier gas). The experimental setup is shown in Figure 7E. Prior to commencing the water-splitting reaction, the mixture was flushed with Ar with a flow rate of 50 mL/min for approximately 90 min to remove any trace of air. The flow was reduced to 25 mL/min during the measurements. Continuous gas flow was controlled by a Bronkhorst mass flow controller.

STH efficiencies were calculated based on average production rates of hydrogen, the Gibbs free energy, the input power, and illuminated area[37]:

$$\eta = \frac{\int \dot{n}_{H_2} dt / \Delta t \cdot \Delta G_r}{P_{sun} A} \quad \text{(Equation 1)}$$

Materials and methods for drop formation and particle synthesis

All chemicals, namely N,N-dimethylformamide (DMF), trifluorotoluene, dichloromethane (DCM), methanol (MeOH) (Sigma-Aldrich), Jeffamine ED900 (J900) (Mw 900 g/mol, Huntsman), fluorinated block of the surfactant FSH (Krytox 157 FSH, Chemours, Wilmington, DE, USA), fluorinated oil HFE-7100 (3M, Chelmsford, MA, USA), and oxalyl chloride (Merck) were used as received.

Surfactant synthesis

Krytox FSH (5 g, 0.71 mmol) is added to a round-bottom flask (RBF) and closed with a septum. DMF (1 drop) is added as a catalyst. 2 mol equiv oxalyl chloride (0.8 mL 2 M solution in DCM, 1.42 mmol) are added dropwise to the RBF, making sure the syringe has previously been flushed with argon. The solution is stirred at room temperature for 3 h to afford a pale yellow, cloudy product. The excess oxalyl chloride is removed under reduced pressure (Hei-VAP, Heidolph, Germany) at 50°C, 1 mbar for 2 h. The activated FSH is dissolved in 10 mL HFE-7100 to obtain a very pale yellow, clear solution. To dry Jeffamine-900, 0.6 mol equiv Jeffamine-900 (0.4 g, 0.43 mmol) is dissolved in 5 mL anhydrous dichloromethane. The Jeffamine-900 solution is added to the activated Krytox and refluxed overnight at 65°C under argon atmosphere to afford a white and cloudy product. The product is dissolved in 2 mL HFE-7100, and 50 mL methanol is added. The solution is centrifuged at 3,000 rcf (relative centrifugal force), 3°C for 15 min (Mega Star, 1.6R, VWR). The supernatant is discarded, and the washing step is repeated three times. The precipitated product is dried under reduced pressure at 1 mbar and 40°C for half an hour and subsequently freeze dried overnight (FreeZone 2.5, Labconco, Kansas City, MO, USA) to afford a produce with white to colorless sticky appearance.

Fabrication of microfluidic device

The mold for the microfluidic device was made using soft lithography.[38,39] The microfluidic devices were produced by mixing PDMS to curing agent (Dow Corning, Midland, MI, USA) at a ratio of 10:1 and cured at 65°C overnight. For the production of single emulsions, the channels were rendered fluorophilic by injecting an HFE-7100-based solution containing 2% trichloro(1H,1H,2H,2H-perfluorooctyl)silane (Sigma-Aldrich, St. Louis, MO, USA) in all the channels for 10 min before drying them with compressed air.

Production of single emulsions

Emulsion drops were produced with a microfluidic flow-focusing device. Single emulsions were produced by injecting the inner phase at 1,000 μL/h using a syringe pump (Cronus Sigma 1000, Labhut, Gloucester, UK). The outer phase was typically injected at 1.5 to 2 times the speed of the inner phase (i.e., 1,500 to 2,000 μL/h).[40]

Synthesis of Rh, La codoped $SrTiO_3$ (STO:Rh,La)

We purchased $SrTiO_3$ from Alfa Aesar (purity 99.0%). STO was mixed in ethanol with 4 mol % La_2O_3 (Sigma Aldrich; purity ≥99.9%), which had been freshly calcined in air at 1,273 K for 12 h and 4 mol % Rh_2O_3 (ABCR; purity 99.9%), and the entire mixture was heated to 1,373 K for 6 h.[30]

Preparation of single emulsion drops

The aqueous phase consisted of 0.1 g STO:Rh,La or WO_3 (Sigma Aldrich; purity 99.9%) photocatalysts suspended in 50 mL aqueous solution of $FeCl_2$ or/and $FeCl_3$ (4.0 mmol/L) for OER and HER half reactions and Z-scheme systems.

The oil phase consisted of HFE-7500 (Novec, 3M Engineering fluid) mixed with 1 wt % FSH_2J900 surfactant. Two methods were used to prepare single emulsion drops: mechanical agitation and microfluidic devices. We mixed the aqueous phase and oil phase at a volume ratio of 1:2 in a glass tube and vortexed this mixture for 1 min to create the emulsion drops by the mechanical agitation.

Pt cocatalyst loading

Pt (2.0 wt %) was loaded by a photodeposition method onto the surface of STO:Rh,La to promote the H_2 evolution reaction. A calculated amount of $H_2PtCl_6.6H_2O$ (Alfa Aesar; purity 99.9%) was added to the aqueous solution of Fe^{2+} (4 mmol/L), and the mixture was subsequently illuminated with visible light. Approximately 5 h were required to complete the Pt photodeposition once it showed stable H_2 evolution. After that, the Xe lamp was turned off, and the experimental solution was again flushed with Ar. Again, the H_2 evolution reaction was carried out onto Pt-loaded STO:Rh,La under visible light.

SUPPLEMENTAL INFORMATION

Supplemental information can be found online at https://doi.org/10.1016/j.xcrp.2023.101755.

ACKNOWLEDGMENTS

The authors would like to thank Dr. Tomasz R. Szymborski (former EPFL) for his initial contribution to the project and Dr. Clemens Suter (EPFL) for his support in the gas analysis and UV-vis measurements. The authors would also like to thank Prof. Dror Noy (Migal-Galilee Research Institute) for initial discussion on drop-based systems. The article is based upon work performed with the financial support of an EPFL's eSeed grant.

AUTHOR CONTRIBUTIONS

S.A.S. and G.D.A. designed and performed the experiments and wrote the paper. S.N. contributed to initial development and photocatalyst material selection and synthesis. S.H. and E.A. conceptualized the research, directed the research, and reviewed the paper.

DECLARATION OF INTERESTS

The authors declare no competing interests.

Received: August 16, 2023
Revised: October 20, 2023
Accepted: November 29, 2023
Published: December 27, 2023

REFERENCES

1. Pinaud, B.A., Benck, J.D., Seitz, L.C., Forman, A.J., Chen, Z., Deutsch, T.G., James, B.D., Baum, K.N., Baum, G.N., Ardo, S., et al. (2013). Technical and economic feasibility of centralized facilities for solar hydrogen production via photocatalysis and photoelectrochemistry. Energy Environ. Sci. *6*, 1983.
2. Takata, T., and Domen, K. (2019). Particulate Photocatalysts for Water Splitting: Recent Advances and Future Prospects. ACS Energy Lett. *4*, 542–549.
3. Wang, Q., and Domen, K. (2020). Particulate Photocatalysts for Light-Driven Water Splitting: Mechanisms, Challenges, and Design Strategies. Chem. Rev. *120*, 919–985.
4. Seitz, L.C., Chen, Z., Forman, A.J., Pinaud, B.A., Benck, J.D., and Jaramillo, T.F. (2014). Modeling practical performance limits of photoelectrochemical water splitting based on

the current state of materials research. ChemSusChem *7*, 1372–1385.

5. Wang, Y., Suzuki, H., Xie, J., Tomita, O., Martin, D.J., Higashi, M., Kong, D., Abe, R., and Tang, J. (2018). Mimicking Natural Photosynthesis: Solar to Renewable H2 Fuel Synthesis by Z-Scheme Water Splitting Systems. Chem. Rev. *118*, 5201–5241.

6. Chen, S., Nandy, S., Vequizo, J.J.M., Hisatomi, T., Nakabayashi, M., Pan, Z., Xiao, Q., Wang, Z., Lin, L., Sun, S., et al. (2023). Promoted Utilization of Charge Carriers in La5Ti2Cu0.9Ag0.1O7S5-Based Photocatalyst Sheets for Efficient Z-Scheme Overall Water Splitting. ACS Catal. *13*, 3285–3294.

7. Nandy, S., Hisatomi, T., Nakabayashi, M., Li, H., Wang, X., Shibata, N., Takata, T., and Domen, K. (2023). Oxide layer coating enabling oxysulfide-based photocatalyst sheet to drive Z-scheme water splitting at atmospheric pressure. Joule *7*, 1641–1651.

8. Nandy, S., Savant, S.A., and Haussener, S. (2021). Prospects and challenges in designing photocatalytic particle suspension reactors for solar fuel processing. Chem. Sci. *12*, 9866–9884.

9. Abe, R., Higashi, M., and Domen, K. (2011). Overall Water Splitting under Visible Light through a Two-Step Photoexcitation between TaON and WO3 in the Presence of an Iodate–Iodide Shuttle Redox Mediator. ChemSusChem *4*, 228–237.

10. Abe, R., Takata, T., Sugihara, H., and Domen, K. (2005). Photocatalytic overall water splitting under visible light by TaON and WO3 with an IO3−/I− shuttle redox mediator. Chem. Commun. 3829–3831.

11. Higashi, M., Abe, R., Takata, T., and Domen, K. (2009). Photocatalytic Overall Water Splitting under Visible Light Using ATaO2N (A = Ca, Sr, Ba) and WO3 in a IO3−/I− Shuttle Redox Mediated System. Chem. Mater. *21*, 1543–1549.

12. Hisatomi, T., Kubota, J., and Domen, K. (2014). Recent advances in semiconductors for photocatalytic and photoelectrochemical water splitting. Chem. Soc. Rev. *43*, 7520–7535.

13. Sasaki, Y., Kato, H., and Kudo, A. (2013). [Co(bpy)3]3+/2+ and [Co(phen)3]3+/2+ Electron Mediators for Overall Water Splitting under Sunlight Irradiation Using Z-Scheme Photocatalyst System. J. Am. Chem. Soc. *135*, 5441–5449.

14. deMello, A.J. (2006). Control and detection of chemical reactions in microfluidic systems. Nature *442*, 394–402.

15. Agresti, J.J., Antipov, E., Abate, A.R., Ahn, K., Rowat, A.C., Baret, J.-C., Marquez, M., Klibanov, A.M., Griffiths, A.D., and Weitz, D.A. (2010). Ultrahigh-throughput screening in drop-based microfluidics for directed evolution. Proc. Natl. Acad. Sci. *107*, 4004–4009.

16. Theberge, A.B., Courtois, F., Schaerli, Y., Fischlechner, M., Abell, C., Hollfelder, F., and Huck, W.T.S. (2010). Microdroplets in Microfluidics: An Evolving Platform for Discoveries in Chemistry and Biology. Angew. Chem. Int. Ed. *49*, 5846–5868.

17. Baret, J.-C. (2012). Surfactants in droplet-based microfluidics. Lab Chip *12*, 422–433.

18. Sklodowska, K., and Jakiela, S. (2017). Enhancement of bacterial growth with the help of immiscible oxygenated oils. RSC Adv. *7*, 40990–40995.

19. Rausch, M.H., Kretschmer, L., Will, S., Leipertz, A., and Fröba, A.P. (2015). Density, Surface Tension, and Kinematic Viscosity of Hydrofluoroethers HFE-7000, HFE-7100, HFE-7200, HFE-7300, and HFE-7500. J. Chem. Eng. Data *60*, 3759–3765.

20. Mohammadi, M.-R., Hadavimoghaddam, F., Pourmahdi, M., Atashrouz, S., Munir, M.T., Hemmati-Sarapardeh, A., Mosavi, A.H., and Mohaddespour, A. (2021). Modeling hydrogen solubility in hydrocarbons using extreme gradient boosting and equations of state. Sci. Rep. *11*, 17911.

21. Aguilar-Cisneros, H., Uribe-Vargas, V., Carreón-Calderón, B., Domínguez-Esquivel, J.M., and Ramirez-de-Santiago, M. (2017). Hydrogen Solubility in Heavy Undefined Petroleum Fractions Using Group Contributions Methods. Oil Gas Sci. Technol. – Rev. D'IFP Energ. Nouv. *72*, 2.

22. Håti, A.G., Szymborski, T.R., Steinacher, M., and Amstad, E. (2018). Production of monodisperse drops from viscous fluids. Lab Chip *18*, 648–654.

23. Etienne, G., Kessler, M., and Amstad, E. (2017). Influence of Fluorinated Surfactant Composition on the Stability of Emulsion Drops. Macromol. Chem. Phys. *218*, 1600365.

24. Etienne, G., Vian, A., Biočanin, M., Deplancke, B., and Amstad, E. (2018). Cross-talk between emulsion drops: how are hydrophilic reagents transported across oil phases? Lab Chip *18*, 3903–3912.

25. Scanga, R., Chrastecka, L., Mohammad, R., Meadows, A., Quan, P.-L., and Brouzes, E. (2018). Click chemistry approaches to expand the repertoire of PEG-based fluorinated surfactants for droplet microfluidics. RSC Adv. *8*, 12960–12974.

26. Gruner, P., Riechers, B., Chacòn Orellana, L.A., Brosseau, Q., Maes, F., Beneyton, T., Pekin, D., and Baret, J.-C. (2015). Stabilisers for water-in-fluorinated-oil dispersions: Key properties for microfluidic applications. Curr. Opin. Colloid Interface Sci. *20*, 183–191.

27. Kato, H., Sasaki, Y., Shirakura, N., and Kudo, A. (2013). Synthesis of highly active rhodium-doped SrTiO3 powders in Z-scheme systems for visible-light-driven photocatalytic overall water splitting. J. Mater. Chem. A *1*, 12327–12333.

28. Murthy, D.H.K., Matsuzaki, H., Wang, Q., Suzuki, Y., Seki, K., Hisatomi, T., Yamada, T., Kudo, A., Domen, K., and Furube, A. (2019). Revealing the role of the Rh valence state, La doping level and Ru cocatalyst in determining the H_2 evolution efficiency in doped $SrTiO_3$ photocatalysts. Sustain. Energy Fuels *3*, 208–218.

29. Konta, R., Ishii, T., Kato, H., and Kudo, A. (2004). Photocatalytic Activities of Noble Metal Ion Doped SrTiO3 under Visible Light Irradiation. J. Phys. Chem. B *108*, 8992–8995.

30. Wang, Q., Hisatomi, T., Ma, S.S.K., Li, Y., and Domen, K. (2014). Core/Shell Structured La- and Rh-Codoped SrTiO3 as a Hydrogen Evolution Photocatalyst in Z-Scheme Overall Water Splitting under Visible Light Irradiation. Chem. Mater. *26*, 4144–4150.

31. Han, L., Lin, M., and Haussener, S. (2017). Reliable Performance Characterization of Mediated Photocatalytic Water-Splitting Half Reactions. ChemSusChem *10*, 2158–2166.

32. Kato, H., Hori, M., Konta, R., Shimodaira, Y., and Kudo, A. (2004). Construction of Z-scheme Type Heterogeneous Photocatalysis Systems for Water Splitting into H2and O2under Visible Light Irradiation. Chem. Lett. *33*, 1348–1349.

33. Zhou, P., Navid, I.A., Ma, Y., Xiao, Y., Wang, P., Ye, Z., Zhou, B., Sun, K., and Mi, Z. (2023). Solar-to-hydrogen efficiency of more than 9% in photocatalytic water splitting. Nature *613*, 66–70.

34. Xing, X., Tang, S., Hong, H., and Jin, H. (2020). Concentrated solar photocatalysis for hydrogen generation from water by titania-containing gold nanoparticles. Int. J. Hydrogen Energy *45*, 9612–9623.

35. Lukes, P., Clupek, M., Babicky, V., and Sunka, P. (2008). Ultraviolet radiation from the pulsed corona discharge in water. Plasma Sources Sci. Technol. *17*, 024012.

36. Zahid, A., Dai, B., Hong, R., and Zhang, D. (2017). Optical properties study of silicone polymer PDMS substrate surfaces modified by plasma treatment. Mater. Res. Express *4*, 105301.

37. Wang, Z., Hisatomi, T., Li, R., Sayama, K., Liu, G., Domen, K., Li, C., and Wang, L. (2021). Efficiency Accreditation and Testing Protocols for Particulate Photocatalysts toward Solar Fuel Production. Joule *5*, 344–359.

38. Arriaga, L.R., Datta, S.S., Kim, S.-H., Amstad, E., Kodger, T.E., Monroy, F., and Weitz, D.A. (2014). Microfluidic Fabrication of Giant Unilamellar Lipid Vesicles with Controlled Microdomain Formation. Biophys. J. *106*, 42a.

39. Xia, Y., and Whitesides, G.M. (1998). Soft Lithography. Angew. Chem. Int. Ed. *37*, 550–575. AID-ANIE550>3.0.CO;2-G.

40. De Angelis, G., Gray, N., Lutz-Bueno, V., and Amstad, E. (2023). From Surfactants to Viscoelastic Capsules. Adv. Mater. Interfaces *10*, 2202450.